JACS
JOURNAL OF THE AMERICAN CHEMICAL SOCIETY

Article

pubs.acs.org/JACS

Evolution of Self-Assembled ZnTe Magic-Sized Nanoclusters

Jun Zhang,*[,†,‡] Clare Rowland,[‡] Yuzi Liu,[‡] Hui Xiong,[‡] Soongu Kwon,[‡] Elena Shevchenko,[‡] Richard D. Schaller,[‡] Vitali B. Prakapenka,[§] Sergey Tkachev,[§] and Tijana Rajh*[,‡]

[†]State Key Laboratory of Heavy Oil Processing, College of Chemical Engineering, China University of Petroleum, Qingdao 266580, P. R. China

[‡]Center for Nanoscale Materials, Argonne National Laboratory, Argonne, Illinois 60439, United States

[§]Center for Advanced Radiation Sources, University of Chicago, Chicago, Illinois 60637, United States

Supporting Information

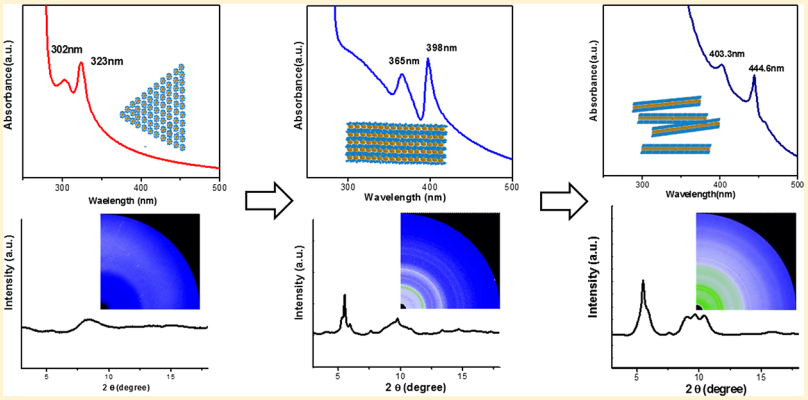

ABSTRACT: Three families of ZnTe magic-sized nanoclusters (MSNCs) were obtained exclusively using polytellurides as a tellurium precursor in a one-pot reaction by simply varying the reaction temperature and time only. Different ZnTe MSNCs exhibit different self-assembling or aggregation behavior, owing to their different structure, cluster size, and dipole−dipole interactions. The smallest family of ZnTe MSNCs (F323) does not reveal a crystalline structure and as a result assembles into lamellar triangle plates. Continuous heating of as synthesized ZnTe F323 assemblies resulted in the formation of ZnTe F398 MSNCs with wurzite structure and concomitant transformation into lamellar rectangle assemblies with the organization of nanoclusters along the ⟨002⟩ direction. Further annealing of ZnTe F398 assembled lamellar rectangles leads to full organization of MSNCs in all directions and formation of larger ZnTe F444 NCs that spontaneously form ultrathin nanowires following an oriented attachment mechanism. The key step in control over the size distribution of ZnTe ultrathin nanowires is, in fact, the growth mechanism of ZnTe F398 MSNCs; namely, the step growth mechanism enables formation of more uniform nanowires compared to those obtained by continuous growth mechanism. High yield of ZnTe nanowires is achieved as a result of the wurzite structure of F398 precursor. Transient absorption (TA) measurements show that all three families possess ultrafast dynamics of photogenerated electrons, despite their different crystalline structures.

INTRODUCTION

Ultrasmall nanoclusters in the size range of 1−2 nm, which contain a defined number of atoms and thus a single size, are often referred to as magic-sized nanoclusters (MSNCs). As a distinct state of matter, MSCNs belong to the interesting intersection region between molecular and larger nanocrystals.[1−9] Owing to the unique structures and/or composition configuration, as well as thermodynamic stability compared to nanocrystals, MSNCs often show exotic chemical and physical properties.[8,10−12] In addition, MSCNs with high-stability and exact same size can form so-called "cluster assembled materials",[13,14] providing a promising approach for the design of nanodevices. Furthermore, many studies have found evidence of correlations between the appearance of MSCNs as intermediates/seeds in the early stage of nanocrystal growth and high uniformity of the final size and shape of nanocrystals.[2,15−18] Consequently, a better understanding of the formation and evolution of MSNCs into nanocrystals would provide insight into the nucleation and growth mechanisms of colloidal nanocrystals and enable rational design of synthesis of nanocrystals with exquisite control of the size and shape of nanoparticles.

Among the various semiconductor materials, ZnTe possesses the lowest electron affinities (negative conduction band (CB): −2.7 eV vs Vac. in bulk with a 2.3 eV band gap) and ultrafast charge separation and transfer dynamics,[19] making it of interest for critically important energy applications. Although many

Received: September 23, 2014
Published: December 22, 2014

DOI: 10.1021/ja509782n
J. Am. Chem. Soc. 2015, 137, 742−749

research papers have been published on MSNCs of metal chalcogenides (CdE; E = S, Se, Te),[7,9,18,20−23] the synthesis and characterizations of ZnTe MSNCs have rarely been reported before,[24] owing to the lack of a suitable synthetic method to satisfy the reaction thermodynamics which are necessary for the formation of ZnTe MSNCs.[20,25] Previous studies have found the combination of a relatively low reaction temperature and high reactivity of precursors to be responsible to a high degree of supersaturation of monomers required for formation of MSNCs.[20,26] The conventional tellurium precursor, trioctylphosphine tellurium (Te-TOP), when reacting with zinc-amine complexes, does not satisfy the reaction kinetics for formation of ZnTe MSCNs, it only results in the regular nanocrystal growth at high temperatures. Groeneveld et al. have developed a synthetic method for ZnTe MSNCs that involves a more reactive zinc source, zinc diethyl.[24] The method generates only a mixture of ZnTe MSNCs, and the isolation of each family of ZnTe MSNCs has not been achieved, despite the fact that access to purified MSNCs is essential for both fundamental studies and exploiting applications of MSNC materials.

Herein, we report a facile and highly reproducible synthetic approach to yield ZnTe MSNCs using polytellurides as a Te precursor. Compared to element tellurium precursor (Te-TOP), polytellurides exist in anionic form and can readily react with zinc cations in solution.[27] The reaction is driven by the nucleophilicity of polytellurides, resulting in a higher concentration of monomers at relatively low temperatures, satisfying the kinetic requirement for ZnTe MSNC formation. By simply tuning the reaction temperature and time, three families of ZnTe MSNCs can be obtained exclusively in a high yield. These ZnTe MSNCs families exhibit different self-assembling behavior while forming hierarchical structures in the presence of excess oleylamine, owing to their different structure, cluster size, and dipole−dipole interactions. Controlling the growth pattern of ZnTe MSNCs, namely step growth and continuous growth, was found to play an important role in determining the diameter and distribution of the ZnTe ultrathin nanowires.

RESULTS AND DISCUSSION

Formation of ZnTe MSNCs and their Quantized (Step) Growth. The ZnTe MSCNs were synthesized by reacting a zinc salt with polytellurides in octadecene (ODE) and/or oleylamine (OAm). Typically, a freshly prepared polytellurides solution was introduced into $ZnCl_2$−OAm complex in ODE preheated to 40 °C followed by heating at elevated temperatures (120 °C−190 °C). The Te precursor was prepared with the addition of superhydride into Te-TOP along with oleylamine. In our previous study, the UV−vis absorption and mass spectrum have confirmed the presence of Te^{2-}, Te_2^{2-}, Te_3^{2-}, and even higher polytellurides, and these species can transform from one to another through equilibrium reactions.[25] Compared to Te-TOP, polytellurides react with a metal source at much milder conditions,[27,28] making a feasible tellurium precursor for synthesis of telluride containing materials. This new precursor allows ZnTe synthesis in a large range of reaction temperatures (80−300 °C) and reaction times (from several minutes to several days), providing an excellent modal system to investigate the earliest stage of NCs nucleation and the shape evolution during the growth.

Absorption spectra of the aliquots taken at various temperatures clearly show that three species can be identified in the heating process, and each species features the appearance of a doublet consisting of sharp absorption peaks (full width at half-maximum within 10 nm, <100 meV) at fixed wavelengths (Supporting Information, Figure S1). The peak positions as well as their relative intensity ratio are highly reproducible for each sample, suggesting that each sample contains only a specific composition/size. The absorption doublets represent two electronic transitions with the lowest energies, the first is from $1S^3/_2(h)$ to 1S(e), and the second from $2S^3/_2(h)$ to 1S(e), in analogy to those reported for CdSe MSNCs.[29,30] These species adopt a discrete step growth pattern that is typically observed for MSCNs, indicating the formation of ZnTe MSCNs. In previous studies, CdSe MSCN families have been named by their primary absorption peak positions in nanometers, such as F395 (Family 395), F463 etc.[20] For convenience, we herein name ZnTe MSCNs in a similar fashion. The smallest species (namely F323) were first formed at 120 °C, featuring two sharp peaks at 323 and 302 nm. As the reaction temperature was elevated to a higher temperature, two additional peaks from a different family of ZnTe MSCNs (F398) appear at longer wavelength (398 and 365 nm) and begin to grow in intensities, while the peaks at 232 and 302 nm still persist, however their intensities begin to wane, suggesting that the F398 family grows at the cost of the F323 family. As the reaction proceeds, peaks at 323 and 302 nm disappear completely and peaks at 398 and 365 nm reach their maximum intensities. When the system was kept at 190 °C, an even larger sized specie (F444) began to form, indicated by the appearance of two peaks at 444 and 400 nm. By extending the reaction time to 50 h at 190 °C, F398 was completely transformed to F444. By simply tuning the reaction temperature and time, all three families of ZnTe MSNCs could be exclusively obtained with high yields as shown in Figure 1 and Supporting Information, Figures s2 and s3).

It is worth noting that there are differences between absorption spectra of ZnTe MSNCs in our study and those from a previously published work.[24] For semiconducting MSNCs, the exact energy of the band gap depends on not only the size (or the exact number of atoms) of the clusters, but also the coordination of the surface influenced by the capping ligands. As a result, the same kind of species synthesized under different synthetic conditions (solvents, surface terminations, capping ligands, and precursors) may have an absorption change as much as 10 nm.[22] Therefore, ZnTe F323 and F398 in our study may be the same species of previously reported 330−333 and 392 families, and F444 is most likely a newly discovered species.

It is plausible that at relatively low temperatures used for initial growth of MSNCs there is not sufficient energy to overcome activation energy of the formation of ZnTe crystallites.[31] It is known from previous studies that formation of free-standing few atom crystallites requires relatively high energies. Therefore, it is more likely for precursors (Zn^{2+}-OAm and Te^{2-}-TOP) at low temperatures to form a kinetically favored structure that does not require dissociation of ions from the stabilizing ligands.[32] A cage-like geometry analogous to those of fullerenes is such a structure that fully incorporates OAm ligands in the cage-like structure.[33] The enhanced stability of these crystals at low temperatures was confirmed using first-principles calculations for $(CdSe)_n$ analogues displaying magic-sized cage-like structures with n = 13, 19, 33, and 34.[33] These isolated MSNCs are centrosymmetric and do not show any Bragg-like diffraction displaying amorphous X-ray diffraction pattern or no presence of fringes in HRTEM

DOI: 10.1021/ja509782n
J. Am. Chem. Soc. 2015, 137, 742−749

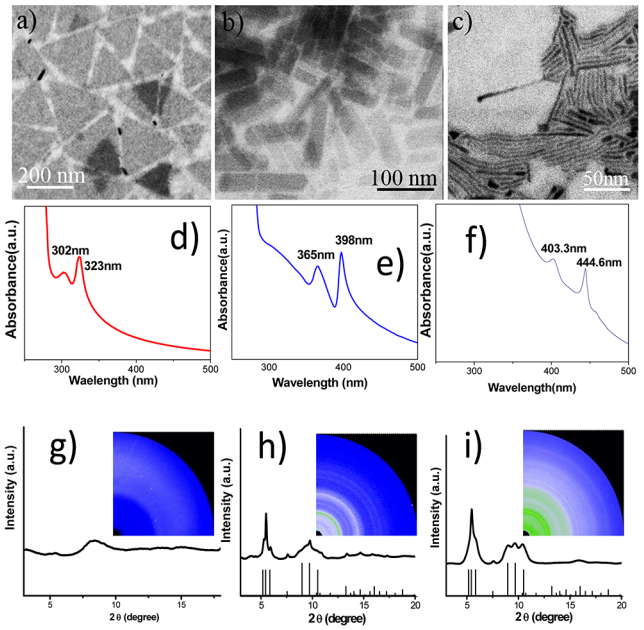

Figure 1. Characterization of various ZnTe MSNCs. (top) TEM images of (a) F323, (b) F398, and (c) F444 assemblies. Images d, e, and f are corresponding absorption spectra of the samples shown in images a, b, and c. Images g, h, and i are synchrotron X-ray diffraction patterns of ZnTe MSNCs in conjunction with line spectrum of wurtzite ZnTe. The insets show corresponding X-ray diffraction 2D patterns.

images. Indeed, the smallest family of MSNCs F323 shows an amorphous structure when exposed to a synchrotron X-ray beam (Figure 1g). However, when exposed to the higher temperatures, a transformation to more stable crystalline structures is expected. After annealing at 190 °C we did observe the appearance of a wurtzite X-ray diffraction pattern (Figure 1h). It should be noted that all diffraction features in the pattern are fairly broad indicating very small crystallite sizes; the diffraction peaks corresponding to the ⟨002⟩ direction are enhanced and narrow, suggesting extended coherence along that direction. This finding is consistent with the appearance of a dipole moment characteristic of a wurtzite ZnTe structure that orients transformed crystallites into extended structures. After prolonged annealing, we observed additional uniform crystallization in all directions and an appearance of crystalline pattern of well crystallized anisotropic structures in F444 (Figure 1i).

Because semiconductor MSNCs are believed to possess a single size and many properties of semiconductor NCs are size-dependent, it would be important to correlate the exact sizes of these ZnTe MSNCs to their superstructure and optical properties. We first tried to use transmission electron microscopy (TEM) to determine the sizes of ZnTe MSNCs. Because of the extreme small sizes (less than 2 nm) and low electron density of MSCNs, the results are inconclusive, especially for the smallest species- F323 (Supporting Information, Figure S2). In our study, matrices assisted laser-deposition-ionization time-of-flight mass spectrometry has also been used to determine the size and composition of ZnTe MSCNs, that for F323 species shows fragments with m/z of 2554 and 3621, which matches well with the clusters of $(ZnTe)_{13}$ and $(ZnTe)_{19}$, respectively (Supporting Information, Figure S4). However, the spectrum of F398 and F444 species as well as that of powdered ZnTe produced identical fragmentation patterns, showing the presence of $(ZnTe)_{13}$ and $(ZnTe)_{19}$ without the appearance of any higher mass clusters. This observation suggests that the results may not be representative of the original clusters of the samples, but the most stable fragments obtained by the laser ablation process. Previously, the size dependence of the band gap has been used to estimate the size of the semiconductor NCs such as CdSe,[34] but data on ZnTe NCs size/band gap dependence are still too limited for accurate determination of the NCs size. This is particularly true for the F323 sample that does not show crystalline behavior and therefore can have a different relationship between the size and band gap energies. A theoretical calculation of confinement energy-size dependence in ZnTe MSNCs, however, can be used to estimate the size of ZnTe clusters that show crystalline behavior.[24,35] For the two families of ZnTe MSNCs (F398 and F444) in this study, the sizes were estimated as 2.3 and 3.37 nm, respectively. It is worth noting that the estimated sizes for F398 and F444 are close to the size estimation by TEM (Figures 3d and 4d).

In Situ Formation of Self-Assembly of ZnTe F323 and F398 MSNCs. ZnTe MSNC assemblies for F323 and F398 families could be formed in situ, when oleylamine was used as the sole solvent for the reaction media. TEM images (Figure 2a,b) of the F323 assemblies show aligned bundles of layered

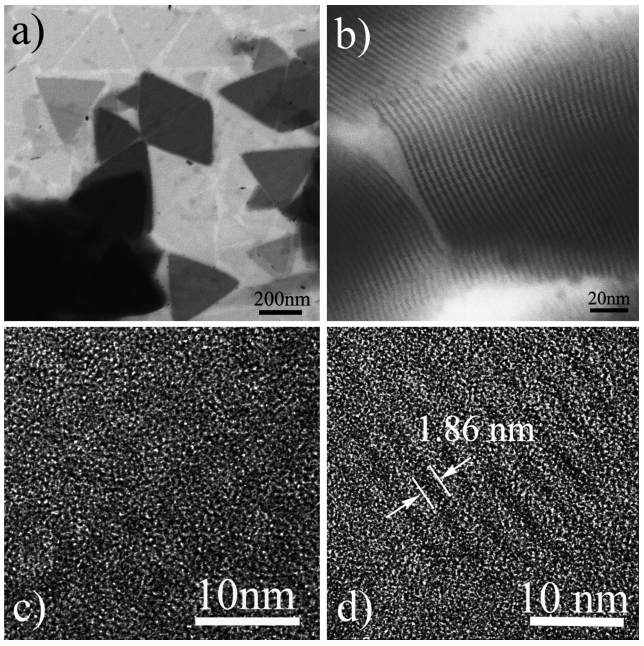

Figure 2. SEM images obtained using transmission electron detector of ZnTe F323 assemblies in various orientation and magnifications: (a) single and multiple layers with horizontal orientation showing triangular shape; (b) vertically orientated bundles of triangular assemblies; (c) HRTEM image of a single layer of assemblies shown in image a; (d) HRTEM image of vertical orientated bundles of assemblies shown in image b, revealing the uniform thickness of the layers.

structures. HRTEM measurements show the space between layers is ~2 nm, which is consistent with the molecular length of oleylamine, while the thickness of the layer approaches 1.86 nm (Figure 2d). This size is in agreement with previously proposed magic-size clusters with cage structures for $(ZnS)_n$ n < 104 that are smaller than 2 nm.[36] The sonication of the

DOI: 10.1021/ja509782n
J. Am. Chem. Soc. 2015, 137, 742−749

product with an excess of toluene resulted in partially dissembling the bundles, forming single-layer plates. The TEM images of horizontally positioned plates show triangle shapes with lateral dimensions ranging from 100 to 300 nm (Figure 2a). Careful HRTEM observation reveals the plates can be characterized as sheets formed by a 2-D monolayer network of assembled ultrasmall nanoparticles (MSNCs) (Figure 2c and Supporting Information, Figure s2). Further HRTEM studies revealed that these plates composed of ultrasmall nanoparticles show no atomic resolved lattice fringes (Figure 2d and Figure s2). The assembled F323 ZnTe MSNCs show a slight red shift and broadening of absorption compared to the discrete components (302 nm vs 300 and 323 nm vs 320 nm) obtained after dissembling in toluene. Both this red shift and peak broadening reflect the interaction between ZnTe MSNCs, resulting from electronic coupling, due to the decrease in particle−particle distance.[37]

These results prompt the question of what is the driving force that causes clusters to assemble. Owing to the strong coordinating effect for the zinc species, oleylamine has been used as capping ligands to control the nanocrystals growth and facilitate the solubility of ZnTe nanoparticles in nonpolar solvents.[38] As the concentration of MSNCs increases during the nucleation as the reaction proceeds, their solubility assisted by the coupling of capping ligands with the free oleylamine is decreasing, due to the declining amount of free oleylamine. To minimize the exposure of capping ligands to the solvent, the particles assemble into a bilayer membrane structure that, upon further increase in the concentration of MSNCs, additionally assembles into multilayer stacking bundles (Scheme 1). As F323 clusters do not have a dipole moment they assemble into crystals whose shape reflects the hexagonal packing and results in a triangular-shaped assembly.

Scheme 1. Schematic Illustration of Evolution of Self-Assembled ZnTe MSNCs

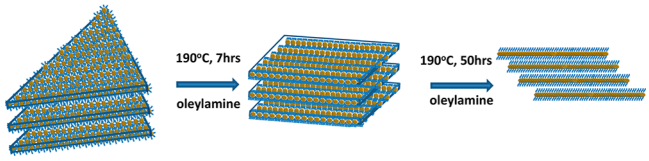

Annealing the assemblies of F323 at 190 °C in oleylamine for 7 h resulted in a formation of F398 assemblies that can be obtained in high purity and yield. The TEM images of the product also show layered bundle structures (Figure 3b, and Supporting Information, Figure S3). However, after reorganization of the bundles, we observed rectangular-shaped nanoplates with lateral dimension of ∼30 nm × ∼100 nm, instead of the starting triangle-shape assembly of F323 before annealing (Figure 3a). To understand the mechanism of this morphology transformation, HRTEM studies of the rectangular nanoplates were performed. Careful observation showed that the rectangle plates also consist of 2-D monolayers of nanoclusters with intralayer spacing of 2 nm corresponding to the length of oleylamine and interlayer spacing of 2.8 nm. This size is for ∼1 nm larger than that observed for the F323 layer thickness. Also, contrary to the F323 MSNCs in triangle nanoplates, the nanoclusters in these rectangle plates did show atomic resolved lattice fringes (Figure 3c,d). Previous studies have predicted that as the MSNCs grow into a larger size, the cage-like structure will transform into crystalline structure due to the

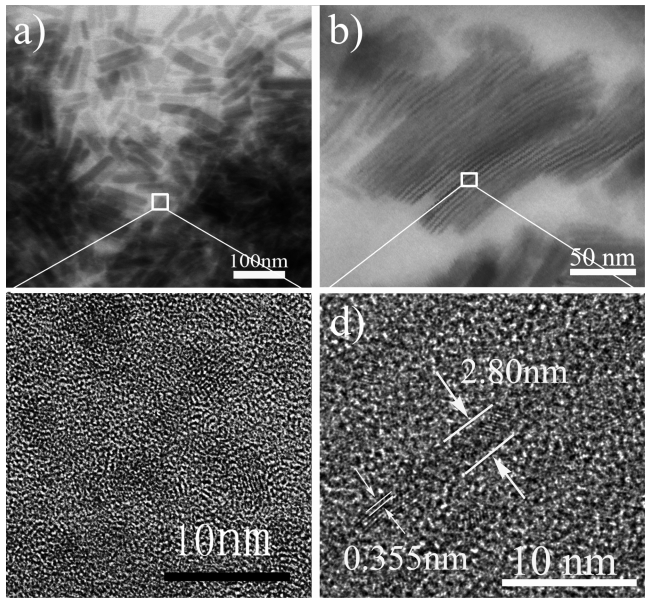

Figure 3. SEM images obtained using transmission electron detector of ZnTe F398 assemblies in various orientations and magnifications: (a) single and multiple layers with horizontal orientation showing rectangular shape; (b) vertically orientated bundles of rectangular assemblies; (c) HRTEM image of a single layer of assemblies shown in image a; (d) HRTEM image of vertical orientated bundles of assemblies shown in image b.

minimization of surface energy.[3] Our results are consistent with this theoretical predication. This is further confirmed using synchrotron X-ray diffraction that shows the appearance of the diffraction pattern characteristic of hexagonal wurzite phase (Figure 1h). Moreover, the pattern shows enhanced signal and narrow features of the ⟨002⟩ direction, suggesting orientation of nanoparticles into periodic arrays of coherent scatterings along this direction. Along with the structure transformation, the interaction between MSNCs changed from isotropic to anisotropic owing to a directional dipole−dipole interaction along *c*-axis (⟨002⟩ direction). As a proof, we observed that purified F398 MSCNs were aligned into a linear pattern when deposited on a TEM grid (Supporting Information, Figure S6b). This also well explains why the overall shape of ZnTe MSCNs assemblies has transformed from triangles into rectangular-shape structures. This macroscopic transformation of assembled nanoparticle morphology is an indication of its microscopic structure. The rectangle shape is intrinsically determined by the existence of dipolar interactions between NCs.

Oleylamine was found to be essential to the formation of ZnTe MSC assembly superstructures. When a combination of OED, oleic acid, and oleylamine was used as reaction medium, while keeping other reaction parameters unchanged, we could still obtain ZnTe MSNCs. However, the resulting ZnTe MSNCs were not well organized into superstructures, showcasing the importance of ligand-solvent interaction in the formation of self-assembled superstructures (Supporting Information, Figure S7). Previous research has demonstrated long-chain amines could form layered structures facilitating the formation of CdSe MSNC bundles.[17,21,26] In our synthesis, we believe oleylamine facilitates the formation of superstructures of ZnTe MSNCs. To explicate the role of oleylamine in ZnTe MSNC superstructure formation, we have studied the zinc−

DOI: 10.1021/ja509782n
J. Am. Chem. Soc. 2015, 137, 742−749

oleylamine complex using small-angle X-ray scattering. As shown in Supporting Information, Figure S8, the pattern clearly shows lamellar structure, indicating that superstructures of ZnTe MSNCs are facilitated by oleylamine through a template effect.

Evolution of Assemblies of F398 into Ultrathin Nanowires (F444). Upon a prolonged annealing time of 10 h at 190 °C for ZnTe F398 assemblies in oleylamine, new red-shifted peaks appear in the optical spectra at 403 and 444 nm, suggesting the formation the next larger sized MSNCs. Indicated by the narrow fwhm (6 nm), the newly formed NCs possess a small size distribution. As the annealing was further prolonged, the intensity peaks at 365 and 398 nm continued to diminish, while the peaks at 403 and 406 nm grow simultaneously, clearly suggesting the F398 MSNCs are converted into larger sized ones rather than a continuous growth. As the annealing time exceeded 50 h, the original peak positions for F398 are completely quenched, leaving behind only absorption features at 403 and 444 nm (Figure 1f). The TEM image (Figure 4b) shows that a majority of the product

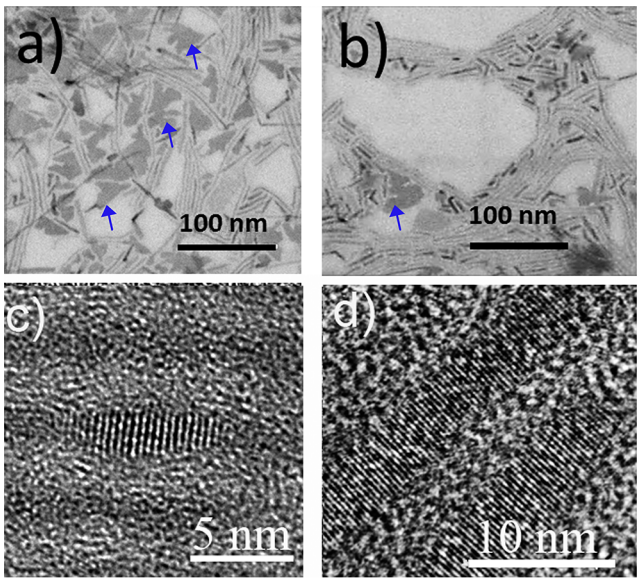

Figure 4. Transformation from ZnTe F398 assemblies (indicated by blue arrows) to ZnTe ultrathin nanowires (F444). SEM images obtained using transmission electron detector (a) after 10 h and (b) after 50 h annealing at 190 °C. Images c and d correspond to HRTEM images of the structures shown in images a and b, respectively.

was transformed into one-dimensional morphology. Several indirect observations suggest ZnTe 1D wires are formed by alignment and fusion of ZnTe nanoclusters during annealing. The HRTEM image of the product obtained at 190 °C for 10 h shows the intermediate stage of the attachment process in which nanoclusters are aligned but have not been fused into a single crystal (Figure 4c). Prolonged annealing time to 50 h at 190 °C transformed the polycrystal nanowires into a perfect single crystal one (Figure 4d and Supporting Information, Figure S9).

The magnitude of the II–VI NCs dipoles was reported to be very high for a hexagonal crystal structure. For example, hexagonal CdSe can have a dipole moment as high as 64 D.[39] Because of this dipole–dipole interaction, the NCs tend to attach and organize along a favored crystallographic axis to form nanowires via oriented attachment as demonstrated by many reports.[40−43] Because the dipole moments of II–VI MSNCs stem from their crystal structure, which is the same for all II–VI semiconductors,[24,44] dipole interaction is expected to play an important role in ZnTe MSNC assembly as well. In our study, as discussed before, F323 MSNCs may lack dipole interaction because of their centrosymmetric "caged structure". Although F398 MSNCs possess a typical wurzite phase as shown by TEM, annealing at the relatively low temperature (190 °C) may not provide enough thermal energy to overcome the stability of MSNC–oleylamine assemblies due to the strong binding ability of oleylamine to the surface of ZnTe nanoclusters.[45] As evidence, when purified and redispersed in toluene, F398 shows a certain degree of attachment by the appearance of wire-like aggregations, while F323 shows irregular aggregation under the same condition (Supporting Information, Figure S6). However, ZnTe F444 MSNCs aggregate through attachment due to strong dipole–dipole interactions between clusters. Taking into account the narrow features in Figure 1h, the attachment occurs along the ⟨002⟩ direction. Under TEM we observed the formation of the wires with crystalline domains matching those of clusters that, after further annealing, convert into single crystalline ZnTe nanowires. Taking into account the increase of the X-ray diffraction peaks associated with directions other than ⟨002⟩ after further annealing (Figure 1i) at this stage, the recrystallization occurs along all directions. Concomitantly, absorption spectra show the step growth pattern during the transformation of F398 assemblies to F444 nanowires in oleylamine, and there is no red shift during the attachment process, indicating that the nanowire retained the width of the MSNCs diameter of 3.7 nm (Figure 4d). Further annealing of the ZnTe nanowire at higher temperature (above 220 °C) will lead to a continuous growth as shown in Supporting Information, Figure S1.

Control of the Competition of Step-Growth and Continuous Growth of F398 MSNCs. Although stepwise growth is a typical growth pattern and has been an indicator of the formation of MSNCs, it is possible to control the competition between stepwise growth and continuous growth patterns of MSNCs. It has been reported that the stepwise growth of MSNCs will switch to the continuous growth when the annealing temperature is above a limit.[24] In our research, we have found that such a growth pattern switch can also be realized by tuning the reaction media composition instead of by changing the temperature. When a certain amount of ODE and oleic acid is introduced in the F398 ZnTe MSNC–oleylamine assemblies while keeping the annealing at 190 °C, the step growth can be outcompeted by continuous growth (Figure 5). Clearly, the presence of oleic acid and ODE initiates the dissolution of some F398 clusters to monomeric species that can react with existing F398 clusters. Because at this temperature formation of clusters with continuous sizes is conceivable, we observe a continuous red shift accompanied by the intensity decrease of F394 absorption peaks as shown in Figure 5a. The continuous growth can keep going on until the size of the resulting NCs is large enough such that no more monomer is produced by dissolution under the reaction condition. The ability of controlling the growth pattern provides us with a facile way to control the size distribution of resulting ZnTe NCs. As shown by both absorption spectra (Figure 5) and TEM images in Supporting Information, Figure S10, the continuous growth of F398 resulted in a much broader size distribution of resulting ZnTe nanocrystals compared to those of step grown. This simple strategy may be extended to

DOI: 10.1021/ja509782n
J. Am. Chem. Soc. 2015, 137, 742−749

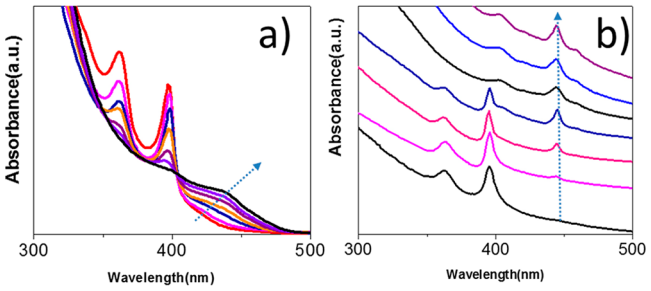

Figure 5. Control of the competition of step-growth and continuous growth of F398 MSNCs: Optical absorption spectra for ZnTe F398 annealed at 190 °C in (a) the mixture of oleylamine, oleic acid, and ODE, showing continuous grow pattern, (b) in pure oleylamine showing step growth pattern.

design the synthetic method for other nanomaterials with narrow size distribution.

Phase Transition during the Growth of F398 MSNCs. Not only the growth pattern, but also the crystalline phase can be controlled during the growth of ZnTe F398 MSNCs. ZnTe has both cubic zinc blende (ZB) and hexagonal wurzite (WZ) structures, and bulk ZnTe with ZB structure is energetically more favorable than that of WZ.[46] In our previous study, ZnTe nanorods with metastabile WZ phase can be obtained by using polytellurides as a Te precursor. To the best of our knowledge, there are no reports on phase control of ZnTe MSNCs, despite the fact that such a control is essential for modulation of the growth pattern of nanocrystals. As shown previously, when ZnTe F398−oleyamine assemblies were annealed with additional oleylamine at 190 °C for 50 h, ZnTe F444 MSCNs with wire-like morphology were obtained, and the XRD study confirms that these ultrathin nanowires retain the WZ phase. On the contrary, when WZ-phased ZnTe F398 MSNCs were annealed at 220 °C for 24 h, a new family of ZnTe MSNCs with the first absorption peak at 446 nm formed (Supporting Information, Figure S11). The XRD study shows that the ZnTe MSCNs possess ZB structure instead of the original WZ (Figure s11a). TEM images of the ZB phased ZnTe F446 show irregular shaped plates instead of ultrathin wires (Figure S11c). It is well-known that the crystalline size has a significant effect on phase transition of II−VI semiconductors.[47] We believe the observed phase transition in ZnTe MSNCs is induced by the small size (3.7 nm) of the nanoclusters at the elevated annealing temperature (220 °C).

Transient Absorption of ZnTe MSNC Assemblies. Transient Absorption of F323 and F398 Assemblies. Spectrally resolved transient absorption measurements performed on hexane suspensions of F323 and F398 using 300 nm excitation, and F444 using 400 nm pump pulses, reveal bleach features with minima at 325, 396, and 446 nm, respectively. For each sample, the observed bleach directly correlates with the static absorption maxima, which suggests a state-filling origin. The bleach line widths appear remarkably narrow with the bleach at 396 nm exhibiting a line width of just 55 meV (roughly twice thermal energy) and are indicative of narrow size distributions. Such bleach line widths suggest either a nanoplatelet morphology, in which, for example, CdSe nanoplates have shown similarly narrow line widths, or highly monodispersed particles. As shown in Figure 6a,b, with increasing pump−probe time delays F323 and F398 exhibit a slight blueshift in the bleach maximum accompanied by the appearance of an induced absorption feature to the red, while

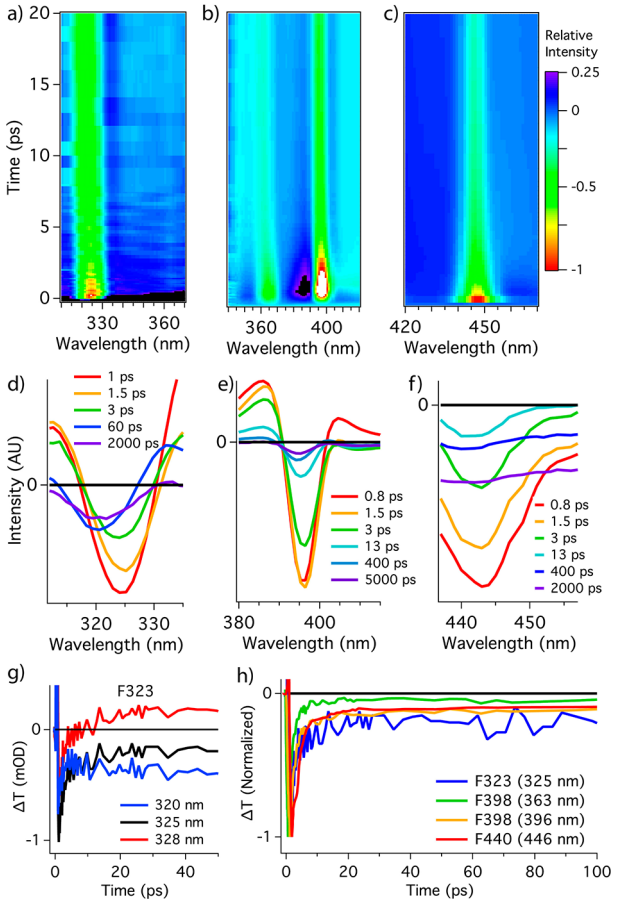

Figure 6. Transient absorption spectra of F323, F398, and F444 are shown in panels a−c, respectively. Spectra are dominated by a bleach that appears strongest at early time and exhibits a slight blueshift at later times, accompanied by the appearance of an induced absorption to the red. In panels d−f, spectra of samples F323, F398, and F444 are shown at several time points, highlighting the evolution and shift of the bleach feature with time. Panels g and h show bleach recovery dynamics of the three prominent features in the spectra at 325, 396, and 446 nm, respectively.

this phenomenon is less pronounced in F444 (Figure 6c). These changes are further highlighted by the derivative shape of the evolving spectra at later times, most prominent in Figure 6d. Dynamics shown in Figure 6g,h for the bleaches at 325, 396, and 446 nm reveal that the significant bleach decays within the first several picoseconds followed by a more long-lived feature. The decay dynamics of a second, less prominent bleach feature in F398 centered at 363 nm appears highly correlated with the redder bleach feature at 396 nm, which suggests a common electronic origin. For each sample, the rapid (picosecond) bleach decay followed by a longer-lived derivative line shape suggests ultrafast electron transfer into proximal accepting states (likely at the surface), probably as a consequence of the small electron affinity of ZnTe,[25] and formation of a longer-lived charge separated state and commensurate Stark shift.

EXPERIMENTAL SECTION

Materials. Trioctylphosphine (TOP, 90%), oleylamine (70%), metal tellurium (Te, 99.999%), zinc chloride, and superhydride ($LiBH(CH_2CH_3)_3$) solution in THF (1 M) were all Aldrich products and used as purchased without further purification. Anhydrous ethanol, chloroform, acetone, and hexane were purchased from

DOI: 10.1021/ja509782n
J. Am. Chem. Soc. 2015, 137, 742−749

various sources. Tellurium-trioctylphosphine (Te-TOP, 1 M for Te) solution was preprepared by dissolving metallic Te into TOP in a glovebox.

Synthesis of ZnTe F323 MSNC Assemblies. All manipulations were carried out using standard Schlenk-line techniques under dry nitrogen. Typically, 0.13 g of zinc chloride was mixed with 10 mL of oleylamine in a 50 mL three-neck flask and was heated to 200 °C under nitrogen gas protection, forming a clear zinc containing solution. The temperature was then dropped to 60 °C. A tellurium precursor which was prepared by mixing Te-TOP solution (0.5 mL), 0.7 M superhydride solution (0.7 mL), and 2 mL of oleylamine was then rapidly injected into the zinc solution. The system temperature was increased to 120 °C by a rate of 10 °C per minute. The reaction was kept at the same temperature for 50 h, before removal of the heating mantel and cooled down to room temperature. The product was separated by centrifuge and redispersed in hexane or toluene.

Synthesis of ZnTe F398 MSNC Assemblies. The procedure was the same as for ZnTe F323 MSNC assemblies, except the as-synthesized ZnTe F323 assemblies were not separated. The system temperature was allowed to increase to 190 °C and was kept at the same temperature for 7 h. The product was separated by centrifuge and redispersed in hexane or toluene.

Transformation of ZnTe F398 Assemblies to Ultrathin ZnTe Nanowires (F444). The as-synthesized ZnTe F398 assemblies in oleylamine were not separated and continued to anneal at 190 °C for 50 h. The product was separated by centrifuge and redispersed in hexane or toluene.

Sample Characterization. TEM images were taken using a transmitted electron detector (TED) on a JEOL 7500 FEG SEM operating at 30 kV. High resolution TEM images were taken on a JEOL 2100F operating at 200 kV. Optical absorption spectra were recorded on a Cary 50 UV−vis spectrophotometer from Varian Inc. Synchrotron X-ray diffraction experiments were carried out at beamline 13-ID-D of GSECARS at the Advanced Photo Source (APS) at Argonne National Laboratory. The transient absorption studies were carried out using a 35 fs amplified Ti:sapphire laser system operating at 2 kHz equipped with an optical parametric amplifier (OPA). A portion of the laser output at 1.55 eV was mechanically time-delayed and focused into a sapphire plate to produce a white light. Pump pulses at 4.1 eV (F323 and F398) and 3.1 eV (F444) were mechanically chopped to 1 kHz and overlapped with the probe pulse on the sample.

CONCLUSION

We have developed a synthetic method for ZnTe MSNCs with high yields. Three distinct ZnTe families with the lowest energy absorption at 323, 398, and 444 nm were obtained separately. By using oleylamine as sole reaction media, lamellar assemblies of F330 and 390 were obtained with high yields. Further annealing ZnTe F398 assemblies in oleylamine resulted in formation of ultrathin ZnTe nanowires. Controlling the growth pattern of ZnTe MSNCs, namely step growth and continuous growth, was found to play an important role in determining the diameter distribution of the ZnTe ultrathin nanowires. Transient absorption (TA) measurements of ZnTe F323, F398, and F444 assemblies all show ultrafast dynamics of photogenerated electrons, despite their different crystalline structures.

ASSOCIATED CONTENT

Supporting Information

TEM images of ZnTe F323, F398, and F444 assemblies; SAXS patterns of ZnTe MSNC assemblies; matrix-assisted laser desorption/ionization−time-of-flight mass spectrum of ZnTe MSNCs; TEM images of aggregation of purified ZnTe MSNCs; TEM images of ZnTe F323 and F398 MSNCs synthesized in the mixed solvent of octadecene and oleylamine; TEM images of ZnTe nanowires obtained by continuous growth and step-growth of F398 MSNCs assemblies. This material is available free of charge via the Internet at http://pubs.acs.org.

AUTHOR INFORMATION

Corresponding Authors

zhangj@upc.edu.cn

rajh@anl.gov

Notes

The authors declare no competing financial interest.

ACKNOWLEDGMENTS

Work at the Center for Nanoscale Materials was supported by the U.S. Department of Energy, Office of Science, Office of Basic Energy Sciences, under Contract No. DE-AC02-06CH11357. Part of the work was performed at GeoSoilEnviroCARS (Sector 13), Advanced Photon Source (APS), Argonne National Laboratory. GeoSoilEnviroCARS is supported by the National Science Foundation−Earth Sciences (EAR-1128799) and Department of Energy−GeoSciences (DE-FG02-94ER14466). J.Z. gratefully acknowledges the financial support from the Center for Nanoscale Materials at Argonne National Laboratory through a CNM distinguished postdoctoral fellowship, National Natural Science Foundation of China (No. 21471160), the Fundamental Research Funds for the Central Universities (14CX05037A), and Tai Shan Scholar Foundation.

REFERENCES

(1) Soloviev, V. N.; Eichhöfer, A.; Fenske, D.; Banin, U. *J. Am. Chem. Soc.* **2001**, *123*, 2354−2364.
(2) Peng, Z. A.; Peng, X. *J. Am. Chem. Soc.* **2002**, *124*, 3343−3353.
(3) Kasuya, A.; Sivamohan, R.; Barnakov, Y. A.; Dmitruk, I. M.; Nirasawa, T.; Romanyuk, V. R.; Kumar, V.; Mamykin, S. V.; Tohji, K.; Jeyadevan, B.; Shinoda, K.; Kudo, T.; Terasaki, O.; Liu, Z.; Belosludov, R. V.; Sundararajan, V.; Kawazoe, Y. *Nat. Mater.* **2004**, *3*, 99−102.
(4) Bowers, M. J.; McBride, J. R.; Rosenthal, S. J. *J. Am. Chem. Soc.* **2005**, *127*, 15378−15379.
(5) Zheng, N.; Bu, X.; Lu, H.; Zhang, Q.; Feng, P. *J. Am. Chem. Soc.* **2005**, *127*, 11963−11965.
(6) Botti, S.; Marques, M. A. L. *Phys. Rev. B* **2007**, *75*, 035311.
(7) Kudera, S.; Zanella, M.; Giannini, C.; Rizzo, A.; Li, Y.; Gigli, G.; Cingolani, R.; Ciccarella, G.; Spahl, W.; Parak, W. J.; Manna, L. *Adv. Mater. (Weinheim, Ger.)* **2007**, *19*, 548−552.
(8) Cossairt, B. M.; Owen, J. S. *Chem. Mater.* **2011**, *23*, 3114−3119.
(9) Wang, Y.; Liu, Y.-H.; Zhang, Y.; Wang, F.; Kowalski, P. J.; Rohrs, H. W.; Loomis, R. A.; Gross, M. L.; Buhro, W. E. *Angew. Chem., Int. Ed.* **2012**, *51*, 6154−6157.
(10) Alivisatos, A. P. *Science* **1996**, *271*, 933−937.
(11) Schreuder, M. A.; McBride, J. R.; Dukes, A. D.; Sammons, J. A.; Rosenthal, S. J. *J. Phys. Chem. C* **2009**, *113*, 8169−8176.
(12) Imaoka, T.; Kitazawa, H.; Chun, W.-J.; Omura, S.; Albrecht, K. *J. Am. Chem. Soc.* **2013**, *135*, 13089−13095.
(13) Claridge, S. A.; Castleman, A. W.; Khanna, S. N.; Murray, C. B.; Sen, A.; Weiss, P. S. *ACS Nano* **2009**, *3*, 244−255.
(14) Qian, M.; Reber, A. C.; Ugrinov, A.; Chaki, N. K.; Mandal, S.; Saavedra, H. M.; Khanna, S. N.; Sen, A.; Weiss, P. S. *ACS Nano* **2009**, *4*, 235−240.
(15) Wang, H.; Tashiro, A.; Nakamura, H.; Uehara, M.; Miyazaki, M.; Watari, T.; Maeda, H. *J. Mater. Res.* **2004**, *19*, 3157−3161.
(16) Jiang, Z.-J.; Kelley, D. F. *ACS Nano* **2010**, *4*, 1561−1572.
(17) Son, J. S.; Wen, X.-D.; Joo, J.; Chae, J.; Baek, S.-i.; Park, K.; Kim, J. H.; An, K.; Yu, J. H.; Kwon, S. G.; Choi, S.-H.; Wang, Z.; Kim, Y.-W.; Kuk, Y.; Hoffmann, R.; Hyeon, T. *Angew. Chem., Int. Ed.* **2009**, *48*, 6861−6864.

DOI: 10.1021/ja509782n
J. Am. Chem. Soc. 2015, 137, 742−749

(18) Evans, C. M.; Love, A. M.; Weiss, E. A. *J. Am. Chem. Soc.* **2012**, *134*, 17298−17305.
(19) Jin, S.; Zhang, J.; Schaller, R. D.; Rajh, T.; Wiederrecht, G. P. *J. Phys. Chem. Lett.* **2012**, *3*, 2052−2058.
(20) Yu, K. *Adv. Mater. (Weinheim, Ger.)* **2012**, *24*, 1123−1132.
(21) Ithurria, S.; Bousquet, G.; Dubertret, B. *J. Am. Chem. Soc.* **2011**, *133*, 3070−3077.
(22) Harrell, S. M.; McBride, J. R.; Rosenthal, S. J. *Chem. Mater.* **2013**, *25*, 1199−1210.
(23) Vossmeyer, T.; Katsikas, L.; Giersig, M.; Popovic, I. G.; Diesner, K.; Chemseddine, A.; Eychmueller, A.; Weller, H. *J. Phys. Chem.* **1994**, *98*, 7665−7673.
(24) Groeneveld, E.; van Berkum, S.; Meijerink, A.; de Mello Donegá, C. *Small* **2011**, *7*, 1247−1256.
(25) Zhang, J.; Jin, S.; Fry, H. C.; Peng, S.; Shevchenko, E.; Wiederrecht, G. P.; Rajh, T. *J. Am. Chem. Soc.* **2011**, *133*, 15324−15327.
(26) Liu, Y.-H.; Wang, F.; Wang, Y.; Gibbons, P. C.; Buhro, W. E. *J. Am. Chem. Soc.* **2011**, *133*, 17005−17013.
(27) Page, E. M. In *Inorganic Reactions and Methods*; John Wiley & Sons, Inc.: 2007; p 41−43.
(28) Page, E. M. In *Inorganic Reactions and Methods*; John Wiley & Sons, Inc.: 2007; p 46−47.
(29) Ekimov, A. I.; Hache, F.; Schanne-Klein, M. C.; Ricard, D.; Flytzanis, C.; Kudryavtsev, I. A.; Yazeva, T. V.; Rodina, A. V.; Efros, A. L. *J. Opt. Soc. Am. B* **1993**, *10*, 100−107.
(30) Norris, D. J.; Bawendi, M. G. *Phys. Rev. B* **1996**, *53*, 16338−16346.
(31) Peng, X. *Adv. Mater. (Weinheim, Ger.)* **2003**, *15*, 459−563.
(32) Harrell, S. M.; McBride, J. R.; Rosenthal, S. J. *Chem. Mater.* **2013**, *25*, 1199−1210.
(33) Corrigan, J. F.; Fuhr, O.; Fenske, D. *Adv. Mater. (Weinheim, Ger.)* **2009**, *21*, 1867−1871.
(34) Murray, C. B.; Norris, D. J.; Bawendi, M. G. *J. Am. Chem. Soc.* **1993**, *115*, 8706−8715.
(35) Li, J.; Wang, L.-W. *Phys. Rev. B* **2005**, *72*, 125325.
(36) Catlow, C. R. A.; Bromley, S. T.; Hamad, S.; Mora-Fonz, M.; Sokola, A. A.; Woodley, S. M. *Phys. Chem. Chem. Phys.* **2010**, *12*, 773−1008.
(37) Döllefeld, H.; Weller, H.; Eychmüller, A. *J. Phys. Chem. B* **2002**, *106*, 5604−5608.
(38) Zhang, J.; Sun, K.; Kumbhar, A.; Fang, J. *J. Phys. Chem. C* **2008**, *112*, 5454−5458.
(39) Shim, M.; Guyot-Sionnest, P. *J. Chem. Phys.* **1999**, *111*, 6955−6966.
(40) Cho, K.-S.; Talapin, D. V.; Gaschler, W.; Murray, C. B. *J. Am. Chem. Soc.* **2005**, *127*, 7140−7147.
(41) Pradhan, N.; Xu, H.; Peng, X. *Nano Lett.* **2006**, *6*, 720−724.
(42) Yu, J. H.; Joo, J.; Park, H. M.; Baik, S.-I.; Kim, Y. W.; Kim, S. C.; Hyeon, T. *J. Am. Chem. Soc.* **2005**, *127*, 5662−5670.
(43) Tang, Z.; Kotov, N. A.; Giersig, M. *Science* **2002**, *297*, 237−240.
(44) Corrigan, J. F.; Fuhr, O.; Fenske, D. *Adv. Mater. (Weinheim, Ger.)* **2009**, *21*, 1867−1871.
(45) Zhang, J.; Chen, P.-C.; Shen, G.; He, J.; Kumbhar, A.; Zhou, C.; Fang, J. *Angew. Chem., Int. Ed.* **2008**, *47*, 9469−9471.
(46) Yeh, C.-Y.; Lu, Z. W.; Froyen, S.; Zunger, A. *Phys. Rev. B* **1992**, *45*, 12130.
(47) Chen, C.-C.; Herhold, A. B.; Johnson, C. S.; Alivisatos, A. P. *Science* **1997**, *276*, 398−401.

DOI: 10.1021/ja509782n
J. Am. Chem. Soc. 2015, 137, 742−749